

An investigation of high pressure COIL performance improvement methods using CFD

Timothy J. Madden

Illinois Univ., Urbana

David L. Carroll

Illinois Univ., Urbana

Wayne C. Solomon

Illinois Univ., Urbana

AIAA, Plasmadynamics and Lasers Conference, 27th, New Orleans, LA, June 17-20, 1996

The chemical oxygen-iodine laser, COIL, presents a significant challenge for analytical models due to the complex couplings between fluid dynamics and chemistry that occur in the system. This paper demonstrates the use of the CFD code GASP as an analytical tool to model these complexities. A conservative, multispecies diffusion model has been developed and added to GASP for molecular transport, and a ten-species, thirteen-reaction finite rate kinetics mechanism is used to describe the nonequilibrium chemistry. The model is used for 3-D Navier-Stokes numerical simulations detailing the mixing and reacting flows within COIL devices at 126 torr total pressure operating conditions. Two injection configurations of a COIL device are considered: a baseline injection scheme and a modification to the baseline scheme designed to improve high pressure performance. A comparison between numerical simulations of the baseline injection scheme at 126 torr and 72 torr total pressure shows that less mixing occurs at high pressure. Detailed comparisons with experimental gain data show very good agreement, validating the model and the approach. The mixing information obtained from the high and low pressure comparison is then used to design a simulation with a modified injection scheme for high pressure operation. The simulation is performed at conditions identical to the original injection scheme and is found to produce a more uniform mixed flow, but with decreased penetration. (Author)

AN INVESTIGATION OF HIGH PRESSURE COIL PERFORMANCE IMPROVEMENT METHODS USING CFD

Timothy J. Madden*

David L. Carroll†

Wayne C. Solomon‡

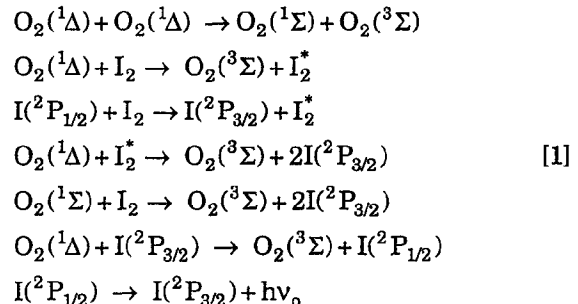
*Department of Aeronautical and Astronautical Engineering, the University of Illinois at Urbana-Champaign,
306 Talbot Lab, Urbana, IL 61801*

Abstract

The Chemical Oxygen-Iodine Laser, COIL, presents a significant challenge for analytical models due to the complex couplings between fluid dynamics and chemistry that occur in the system. This paper demonstrates the use of the Computational Fluid Dynamics (CFD) code GASP as an analytical tool to model these complexities. A conservative, multi-species diffusion model has been developed and added to GASP for molecular transport, and a ten specie, thirteen reaction finite rate kinetics mechanism is used to describe the non-equilibrium chemistry. The model is used for three-dimensional Navier-Stokes numerical simulations detailing the mixing and reacting flows within COIL devices at 126 torr total pressure operating conditions. Two injection configurations of a COIL device are considered: a baseline injection scheme and a modification to the baseline scheme designed to improve high pressure performance. A comparison between numerical simulations of the baseline injection scheme at 126 torr and 72 torr total pressure shows that less mixing occurs at high pressure. Detailed comparisons with experimental gain data show very good agreement, validating the model and the approach. The mixing information obtained from the high and low pressure comparison is then used to design a simulation with a modified injection scheme for high pressure operation. The simulation is performed at conditions identical to the original injection scheme and is found to produce a more uniform mixed flow, but with decreased penetration.

I. Introduction

The COIL^{1,2,3} is a high-power, short wavelength chemical laser. The COIL uses a series of chemical reactions to produce electronically excited atomic iodine, the source of radiative and stimulated emission. A two phase exothermic reaction between basic hydrogen peroxide (BHP) and Cl₂ produces the singlet delta electronically excited state of molecular oxygen O₂(¹Δ). This occurs in the O₂(¹Δ) generator, Figure 1. O₂(¹Δ) diffuses from the BHP liquid into a carrier gas flow that travels through the device. Molecular iodine is injected into the gas flow, and through a series of electronic-vibrational collisional energy transfers, I₂ is dissociated producing ground-state I, I(²P_{3/2}). A resonant collisional energy transfer from O₂(¹Δ) to I(²P_{3/2}) produces the electronically excited I(²P_{1/2}). I(²P_{1/2}), also denoted as I*, emits a photon at a wavelength of 1.315μm to provide the lasing energy in the COIL. The gas phase chemistry that drives the COIL can be summarized as:



II. Background

The CFD code used in the simulation of the COIL is GASP version 2.2⁴ released by AeroSoft, Inc. GASP discretizes the integral form of the Reynolds Averaged Navier Stokes and species

* Student member AIAA.

† Member AIAA.

‡ Member, associate fellow AIAA.

Copyright © 1996 by the American Institute of Aeronautics and Astronautics, Inc. All rights reserved.

continuity equations using a finite volume formulation. The resulting set of algebraic equations are solved using 3 factor approximate factorization. Coupled to these equations are closure models for molecular transport properties and Arrhenius type finite rate chemical kinetics.

The low magnitude 10^3 to 10^4 Reynolds numbers of COIL operation create conditions under which diffusive molecular fluxes dominate mixing processes. For this reason, a conservative, detailed diffusion model⁵ was added to the GASP code to calculate the individual species diffusive fluxes, replacing the existing constant Schmit number based Fick's law model. The model is given by the equation

$$\rho_i \bar{v}_i = -n m_i D_{im} \left[\frac{\partial \chi_i}{\partial \bar{r}} + (\chi_i - f_i) \frac{\partial \ln P}{\partial \bar{r}} \right] + f_i n \sum_{j=1}^N m_j D_{jm} \left[\frac{\partial \chi_j}{\partial \bar{r}} + (\chi_j - f_j) \frac{\partial \ln P}{\partial \bar{r}} \right] \quad [2]$$

where $\rho_i \bar{v}_i$ is the diffusive flux for each species, n is the molar concentration, m_i is the molecular weight, D_{im} is the effective mixture diffusion coefficient for each species, P is the pressure, and χ_i and f_i are the mole and mass fractions.

III. Approach

The general approach to simulating the COIL was to reduce the problem such that detailed features necessary for accuracy could be retained without overwhelming the available computational facilities. The first reduction was made by simulating the COIL nozzle from the injector region to a point past the mirrors, using diagnostic data from experiments (see Fig. 1) to provide the inflow conditions. This allows the generator and transition duct upstream of the mixing nozzle to be removed from the simulation. Instead of simulating the entire width of the COIL mixing and reacting flowfield, a single injector set was isolated from a row of geometrically similar injector sets and was modelled in detail. Geometric symmetry about the centerline of the COIL mixing nozzle and within the injector set was also used to further reduce the size of the computational domain (see Fig. 2). The chosen computational domain was then discretized using a 108x26x16 cell grid.

Having established the computational domain, a zonal approach to the fluid dynamics based upon the character of the flow in that region was

developed. The first zone was fixed to encompass the injector mixing region through the throat to fully supersonic flow. The second zone begins where the first ended and continues to the exit plane of the domain. The fluid dynamics within the first zone are described using the full Navier-Stokes equations since the flowfield holds both sub- and transonic regions. The second zone uses the parabolized Navier-Stokes equations to describe the fluid dynamics since the flow is fully supersonic.

Radiation transport modelling, necessary for simulating COIL operation with power extraction, is neglected here since comparisons with experiment are made with zero power gain data. It is then assumed that data sufficient for determining the influence of pressure upon the COIL can be extracted from the simulation by modelling only the gas dynamics, molecular transport, and chemistry.

The flow rates, pressures, temperatures, and species concentrations used are taken directly from the experimental diagnostics, maintaining a one-to-one comparison with experiment. This information is input into the simulation through the inflow boundary conditions. Table 1 lists this information. The actual injector diameter that is simulated is reduced from the original diameter of .032" to account for boundary layer growth. This adjustment is made by using a discharge coefficient of .65. The discharge coefficient for this device is determined by the ratio of the measured mass flow to the ideal mass flow for choked flow. The COIL chemistry is modelled using a 10 specie, 13 reaction finite rate mechanism developed by Carroll⁶. All rates used in this mechanism are experimentally measured values.

IV. Data Analysis

The presentation of data occurs as follows: high pressure data for the baseline injection cases are shown and then compared to data from a low pressure simulation for the same configuration. Next, a high pressure simulation of a modified injection configuration is compared to the high pressure simulation of the baseline configuration.

IV.1. Simulation of High Pressure COIL Operation - Original Injection Scheme

3-D perspective plots for the baseline high pressure ($P=126$ torr) simulation are shown in Figs. 3 through 9. Figs. 3 and 4 show the I_2 mole fraction plots in this perspective. The gas injected

from the large hole turns over and penetrates to the centerline and spreads as it collides with gas from its opposite across the centerline. The gas from the small injectors mixes into regions which the large injectors do not affect. The gas from the injectors fills much of the nozzle, but sharp gradients in concentration exist past the 8.0 cm plane indicating incomplete mixing. The area between the small injectors along the $y=0.0$ cm plane suggests the need for an improved mixing scheme as evidenced by the region of low I_2 concentration which persists to the exit plane, although most of the I_2 is dissociated at this point.

Figs. 5 and 6 show the mixing from the opposite perspective, i.e. the concentrations of the $O_2(^1\Delta)$ in the flow. The core injectant flow is clearly visible in Fig. 5 as it contrasts with the high concentrations of $O_2(^1\Delta)$ in the primary. The reaction zone develops as a band of low $O_2(^1\Delta)$ concentration and spreads as $O_2(^1\Delta)$ is used. Fig. 6 shows that sharp differences in $O_2(^1\Delta)$ concentration exist at all planes in the second zone, including the exit plane. The dark regions indicate un-mixed $O_2(^1\Delta)$ whereas the lighter regions indicate near complete usage of $O_2(^1\Delta)$. As evidenced by the dark, high $O_2(^1\Delta)$ concentration contours in the exit plane, much of the energy potential of the $O_2(^1\Delta)$ is not accessed.

	Primary Flow	Secondary (Injectant) Flow
T_0 (K)	282.4	434.8
P_0 (torr)	126.7	541.6
Mach Number	0.644	1.0
U (m/sec)	365.1	817.2
Yield	0.66	0.0
Molar Flow Rates (mole/s)		
$O_2(^3\Sigma)$	0.146	0.0
$O_2(^1\Delta)$	0.318	0.0
H_2O	0.10	0.0
Cl_2	0.0725	0.0
I_2	0.0	0.015
He	5.0	1.35

Table 1. Flow conditions for GASP simulation of a COIL device at 126 torr stagnation pressure.

IV.2. Comparison of High and Low Pressure COIL Operation - Original Injection Scheme

The small signal gain, or gain as it commonly referred to, appears in Figs. 7 and 8. The gain is

a parameter that is used to measure the potential for extraction of radiative energy from the flow as indicated by the number densities of I^* and I . The concentration of I^* indicates the number of atoms capable of releasing photons and the concentration of I represents the number of atoms capable of absorbing photons. The gain is described by the equation

$$g = \frac{7}{12} \left(\frac{A\lambda^2}{8\pi} \right) \Phi(\nu) \left(N_{I^*} - \frac{1}{2} N_I \right) \quad [3]$$

where $A=5.0\text{sec}^{-1}$, $\lambda=1.31527 \times 10^{-4}\text{cm}$, and N_{I^*} and N_I are the number densities of I^* and I , and $\Phi(\nu)$ is the Voight lineshape function. Although the gain plots show the potential for the extraction of photons from the flow as far upstream as the throat, the highest levels of gain appear downstream. Peak gains occur along the nozzle centerline with values remaining above $.01\text{ cm}^{-1}$ from the 5 cm plane to the exit of the nozzle. Following the trends noted in the I_2 and $O_2(^1\Delta)$ plots, the gain distribution is seen to have strong 3D variation, especially in the y and z directions indicating incomplete mixing. This contrasts with the gain distribution from a previous simulation of the same COIL mixing nozzle at 72 torr total pressure⁷. The gain distribution in the lower pressure case found in Figs. 9 and 10 shows that the peak gain is spread more uniformly in the y direction, indicating good mixing.

	Primary Flow	Secondary (Injectant) Flow
T_0 (K)	300.4026	435.12
P_0 (torr)	72.015	291.10
Mach Number	0.644	1.0
U (m/sec)	345.642	811.23
Yield	.50	0.0
Molar Flow Rates (mole/s)		
$O_2(^3\Sigma)$	0.2307	0.0
$O_2(^1\Delta)$	0.2307	0.0
H_2O	.10	0.0
Cl_2	.0385	0.0
I_2	0.0	.0075
He	1.5	.65

Table 2. Flow conditions for GASP simulation of a COIL device at 72 torr stagnation pressure.

An explanation for this behavior can be found by examining the equation for the binary diffusion

coefficients D_{ij} from equation 8.2-44 of Hirschfelder et al⁸:

$$D_{ij} = .018829 \frac{\sqrt{T^3 \left(\frac{1}{m_i} - \frac{1}{m_j} \right)}}{P \sigma_{ij}^2 \Omega_{ij}} \quad [4]$$

where T is the temperature, σ_{ij} is the collisional cross section, and Ω_{ij} is the collision integral. Examining this equation, it is immediately evident that when molecular diffusive transport dominates mixing processes in flowfields with similar compositions and temperatures, the pressure is the primary determinant of mixing. Thus high pressure COIL operation can be expected to have less mixing than low pressure operation for the same device.

IV.3. Comparison of the High Pressure COIL Operation Simulation with Experimental Data

The gain data⁹ from the high pressure simulation is compared with experimental data for the same COIL device and flow conditions, Fig. 11. To compare the data, the pointwise gain must be averaged to match the manner in which the experimental data was taken. The average gain is given by the equation

$$g_{ave}(v, x, z) = \frac{1}{L} \sum_{j=2}^{N_y} \frac{1}{2} [g(v, x, y_{j-1}, z) + g(v, x, y_j, z)] [y_j - y_{j-1}] \quad [5]$$

where L is the width of the simulation along the y axis and N_y is the number of points in the y direction. This is the gain that is measured by the experimental diagnostic where a very low intensity laser beam is passed through the media along a path parallel to the y axis to measure the average gain. The comparison between the high pressure average gain and the experimentally measured gain is illustrated in Fig. 11. The plots at the different streamwise positions show that there is very good agreement between the experiment and simulation data.

IV.4. Simulation of High Pressure COIL Operation - New Injection Scheme

The high pressure case examined previously suggested a modification of the injection scheme to improve the primary/secondary mixing. The

areas of un-mixed $O_2(^1\Delta)$ in the high pressure case were primarily centered about the midpoint between the large injectors, suggesting the addition of injector holes at these positions to improve the mixing. A numerical experiment incorporating this logic was developed to investigate the effect of modifying the injection scheme upon the high pressure operation of the COIL. In this calculation the additional large injectors were added at the midpoint between the large injectors; the number and placement of small injectors remained the same. To provide a direct comparison with the original injection scheme, the diameter of the large injector was reduced to 0.023" from the original 0.032" to give the same secondary mass flow rates. A comparison of the two injection schemes is given in Fig. 12. The actual diameter used for the injector inflow boundary condition was determined using the same discharge coefficient (0.65) as with the original high pressure case.

The modification to the injection scheme changes the geometric symmetry of the injectors. This allows symmetry boundary conditions to be applied in planes at the centerline of the large injector and the centerline of the small injector. All other boundary conditions with the exception of the size of the large injector remain the same. The operating conditions used as input to the original high pressure case are used as input for this case as well (see Table 1).

3D perspective plots for the modified injection scheme are found in Figs. 13 through 16. The I_2 mole fraction appearing in Figs. 13 and 14 shows that the desired affect is achieved, i.e. a more uniform mixed flow. The regions between the injectors are well mixed giving a relatively uniform I_2 distribution across the nozzle. However, penetration of the I_2 jets into the primary flow is not optimum, however, with penetration to about 2/3 the distance to the nozzle centerline was obtained. $O_2(^1\Delta)$ mole fractions plots are shown in Figs. 15 and 16 and show that all $O_2(^1\Delta)$ between the injectors is used as a result of the improved lateral mixing. On the other hand with the penetration not optimum, $O_2(^1\Delta)$ near the nozzle centerline remains un-accessed.

IV.5. Simulation of High Pressure COIL Operation - Comparison of New and Old Injection Schemes

A comparison of the gain distribution from the original injection case and that from the new injection is shown in Figs. 17a-d. The injection

schemes can be compared by noting the injector locations in Figs. 17a,c. The first feature that is evident in comparing the two cases is the decrease in penetration with the decrease in the diameter of the large injector. The new injection scheme penetrates approximately half as far as does the original scheme, and thus does not reach the vertical centerline of the nozzle. However, the new injection scheme does show considerably better lateral mixing than the original injection scheme. Figs. 17c,d show a more uniform distribution of gain in the y axis direction when compared to the large gaps in the gain that appear in Figs. 17a,b for the original scheme. The decrease in penetration with the new injection scheme limits the gain region in the vertical direction to the upper 75% of the nozzle as compared to the wall to centerline distribution of the gain in the original injection case. This shortcoming may be offset by higher peak gain and better lateral spread with the new injection scheme. Peak gains with the new injection scheme are above 1.8%/cm whereas the original injection scheme produced peak gains of approximately 1.5%/cm. Also, the lateral spread occurs much faster and is more uniform with the new injection scheme; note the transverse fill occurring before the 4 cm plane. In the original injection scheme, complete mixing in the y direction does not occur until after the 6 cm plane. The improved mixing indicates that more $O_2(^1\Delta)$ is accessed with the new injection scheme; consequently higher gain occurs.

V. Summary and Conclusion

Detailed information about the mixing and reacting flowfield of a COIL has been provided by numerical simulation. Plots of the I_2 and $O_2(^1\Delta)$ mole fractions and gain predicted by a simulation of a 126 torr stagnation pressure COIL indicate that mixing is incomplete. The plots show that a gap exists between the injector sets where significantly less chemical reaction occurs. Little or no I_2 mixes into this area and less $O_2(^1\Delta)$ is used, if at all. The end result is significantly lower gain and strong variation in gain along the optical axis. A comparison with the gain from a simulation of the same COIL device at 72 torr stagnation pressure operation shows that this phenomenon does not occur at lower pressures. The low pressure gain profile is more uniform indicating better mixing between the injector sets.

The operational pressure of the COIL device was shown to be the scaling factor of molecular diffusive mixing within a COIL through the $1/P$

dependence of the binary diffusion coefficients. If molecular diffusion is the primary mechanism for mixing within a COIL device, then the operational pressure will directly affect the mixing and performance. Two alternatives exist for modifying the mixing within a COIL device. The first is to modify the spacing between injectors to change the mixing, molecular diffusion remaining the primary mixing agent. The second is to use other mixing mechanisms such as swirl or vortex inducement to change the mixing characteristics. It should be cautioned that mixing improvement does not necessarily equate with performance improvement in a COIL. Other factors such as $O_2(^1\Delta)$ usage and I^* deactivation are influenced by the mixing rates and should be carefully considered as well, so that the energy potential is not lost before power extraction can occur.

The logical application of the model and approach described here is the optimization of a COIL device. The detailed information provided by the simulations shown here can be used to qualitatively and quantitatively gauge mixing within a COIL at different operating conditions and different configurations. This mixing information can then in turn be used to guide the sizing and placement of injector orifices as was shown here. A suggested future investigation using this approach would be the simulation of a high pressure COIL device with other modifications to the injection scheme. Mass flow rates and flow conditions for these suggested simulations would be identical to those of the 126 torr stagnation pressure simulation listed in Table 1, such that a one-to-one comparison could be made between the cases.

Acknowledgments

This work was supported by the U. S. Air Force through Logicon/RDA subcontract 907629. This work was supported in part by a grant of HPC time from the DoD HPC Shared Resource Center on the CEWES Cray C916. The authors thank L. Sentman, G. Hager, D. Plummer, and P. Crowell for their time and suggestions during this work.

References

- ¹ McDermott, W. E., Pchelkin, N. R., Benard, D. J., and Bousek, R. R., "An Electronic Transition Chemical Laser," *Applied Physics Letters*, 32, No. 8, pp. 469-470, (1978).

² Hager, G. D., "COIL-IV, A Chemical Oxygen-Iodine Laser," Air Force Weapons Lab Technical Report 85-64, Air Force Weapons Lab, Kirtland AFB, NM.

³ Truesdell, K. A., Lamberson, S. E., and Hager, G. D., "Phillips Laboratory COIL Technology Overview," 23rd AIAA Plasmadynamics and Lasers Conference, AIAA 92-3003, July, 1992.

⁴ McGrory, W. D., Slack, D. C., Applebaum, M. P., and Walters, R. W., "GASP Version 2.2 The General Aerodynamic Simulation Program," AeroSoft Inc., Blacksburg, VA, (1993).

⁵ Bird, R. B., Stewart, W. E., and Lightfoot, E. N., *Transport Phenomena*, John Wiley & Sons, 1962, pp. 571.

⁶ Carroll, D. L., "Modeling High-Pressure Chemical Oxygen-Iodine Lasers," *AIAA Journal*, **33**, No. 8, pp. 1454-1462, (1995).

⁷ Madden, T. J., "Detailed Investigation of Mixing in COIL Devices using CFD," Ph.D. dissertation, University of Illinois at Urbana-Champaign.

⁸ Hirschfelder, J. O., Curtiss, C. F., and Bird, R. B., *Molecular Theory of Gases and Liquids*, John Wiley & Sons, 1954, pp. 539.

⁹ Tate, R. F., Hunt, B. S., Helms, C. A., Hager, G. D., and Truesdell, K. A., AIAA Paper 94-2438, 1994.

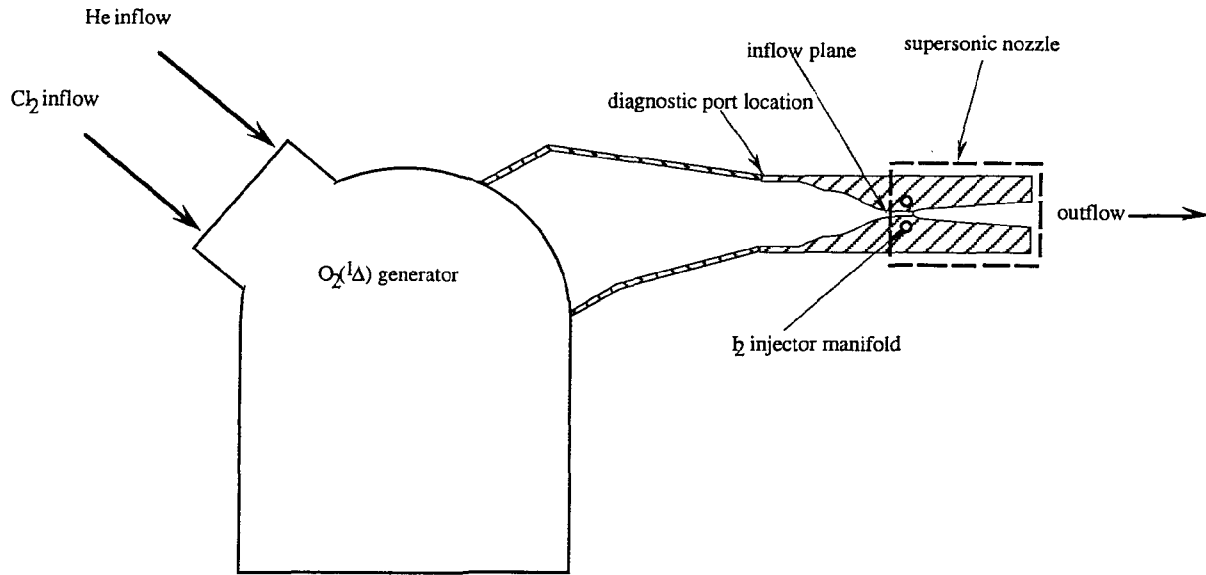


Figure 1. Diagram of a generic COIL device.

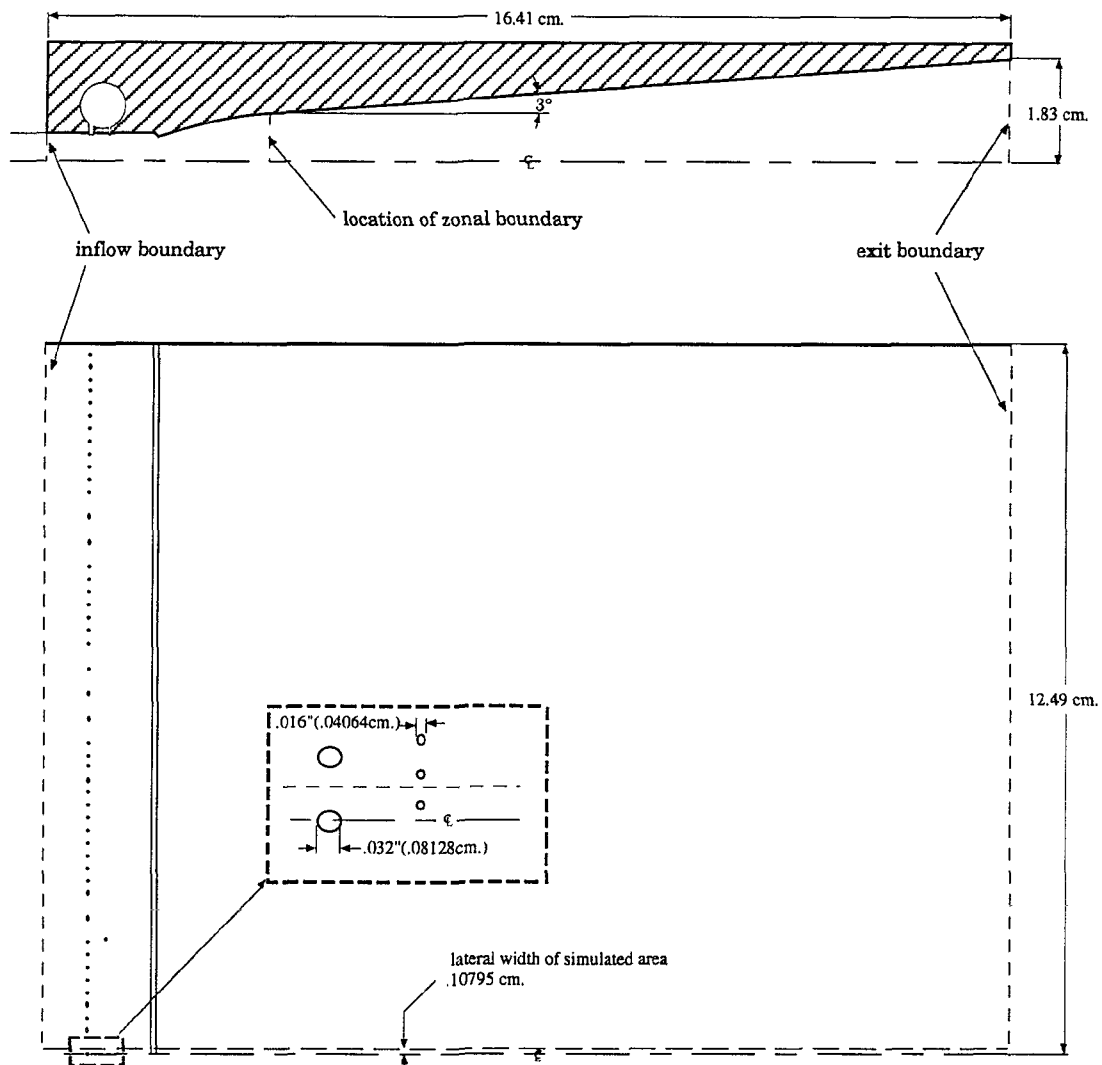


Figure 2. Diagram of COIL mixing nozzle and the computational domain.

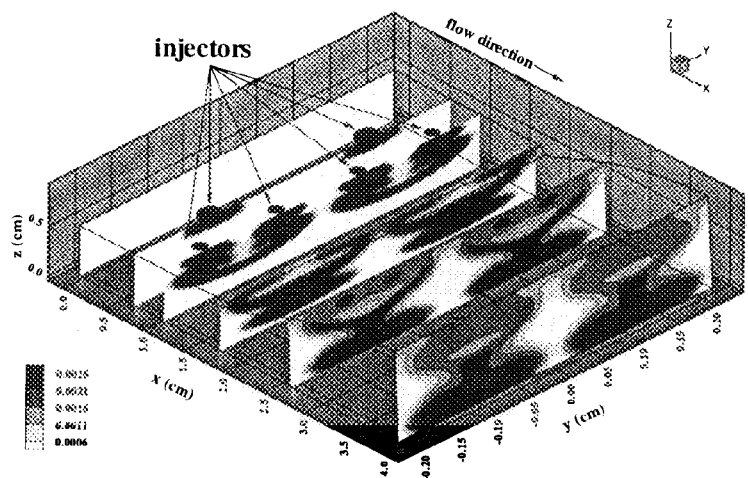


Figure 3. I₂ mole fraction in Zone 1, baseline injection, 126 torr.

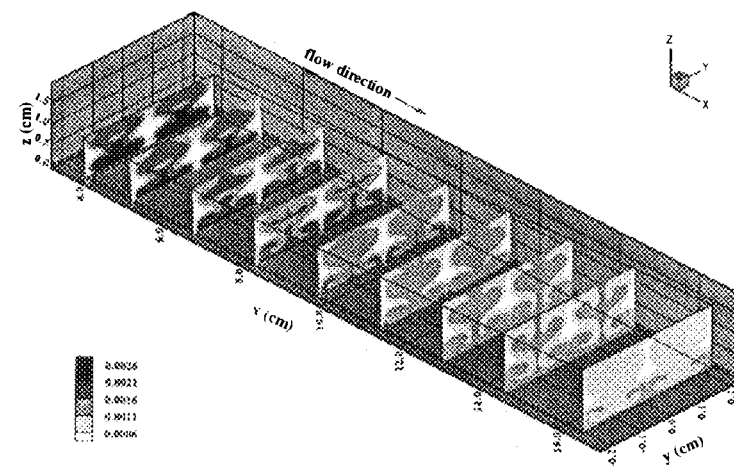


Figure 4. I₂ mole fraction in Zone 2, baseline injection, 126 torr.

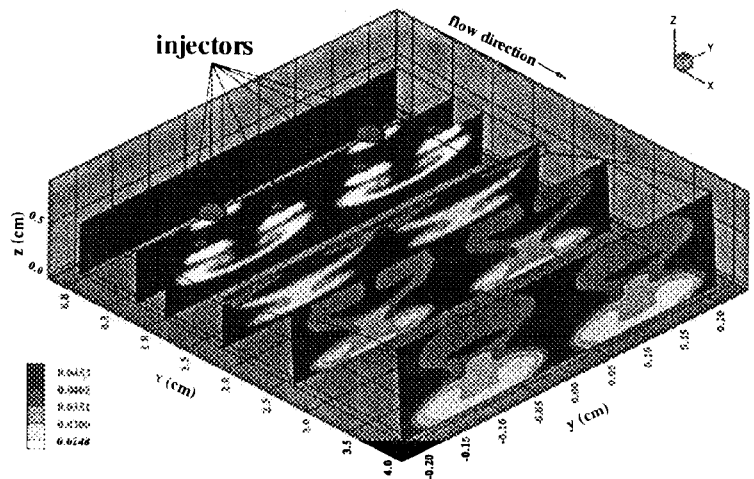


Figure 5. O₂(¹Δ) mole fraction in Zone 1, baseline injection, 126 torr.

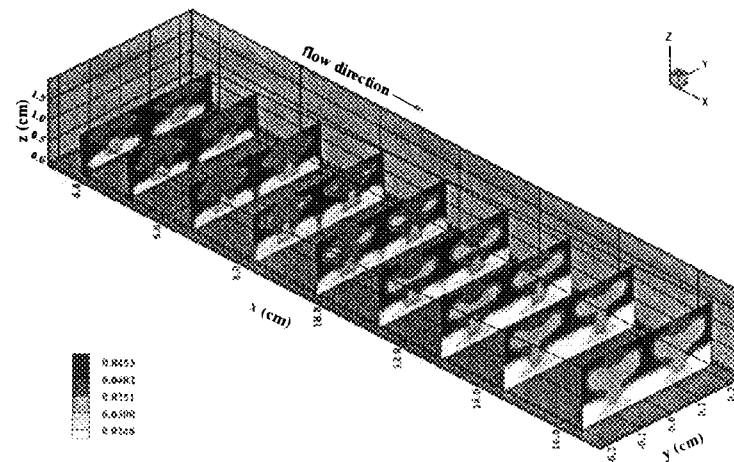


Figure 6. O₂(¹Δ) mole fraction in Zone 2, baseline injection, 126 torr.

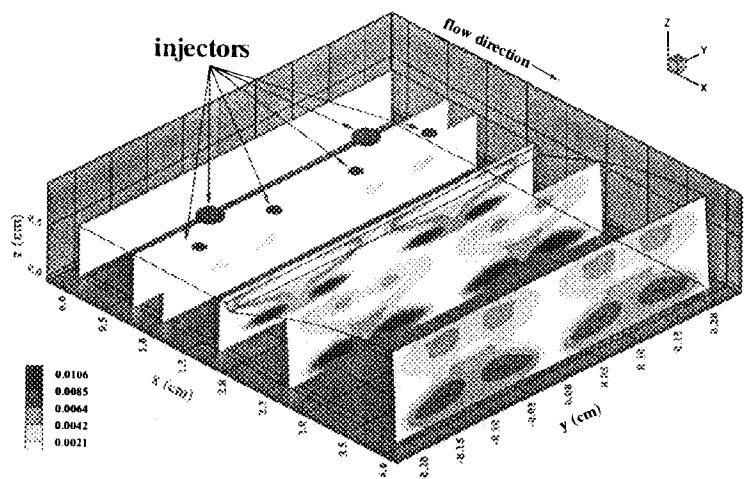


Figure 7. Gain (cm^{-1}) in Zone 1, baseline injection, 126 torr.

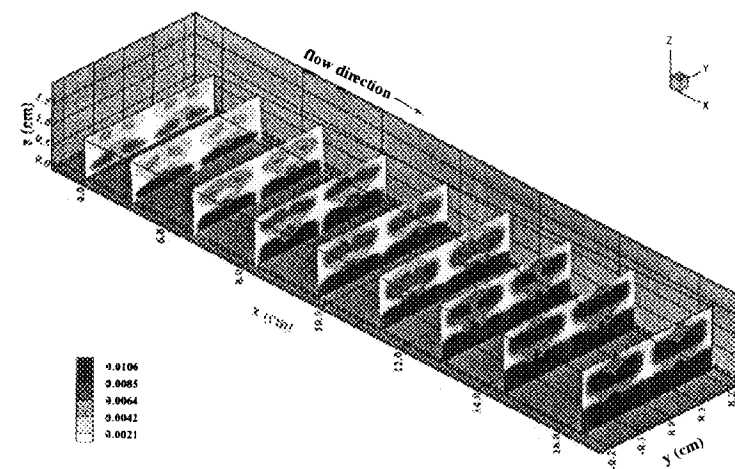


Figure 8. Gain (cm^{-1}) in Zone 2, baseline injection, 126 torr.

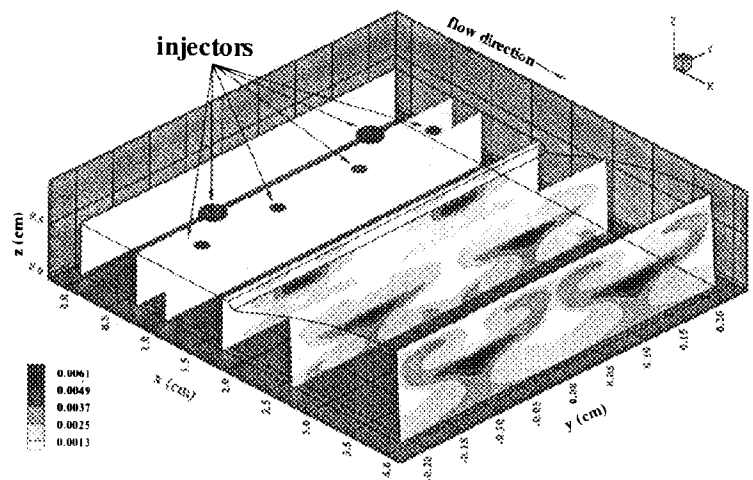


Figure 9. Gain (cm^{-1}) in Zone 1, baseline injection, 72 torr.

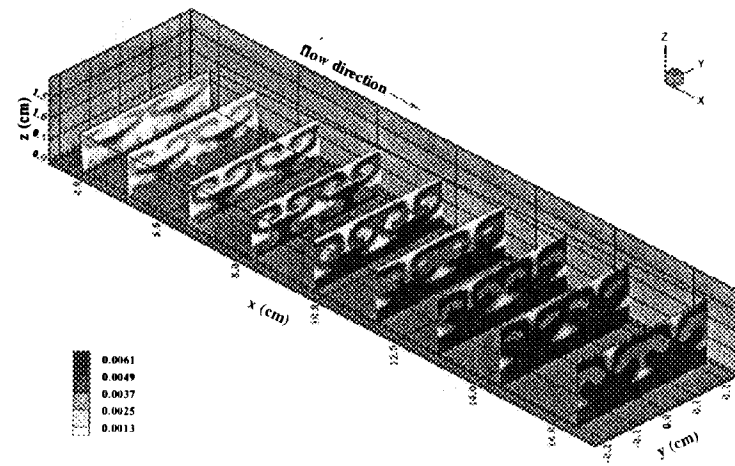


Figure 10. Gain (cm^{-1}) in Zone 2, baseline injection, 72 torr.

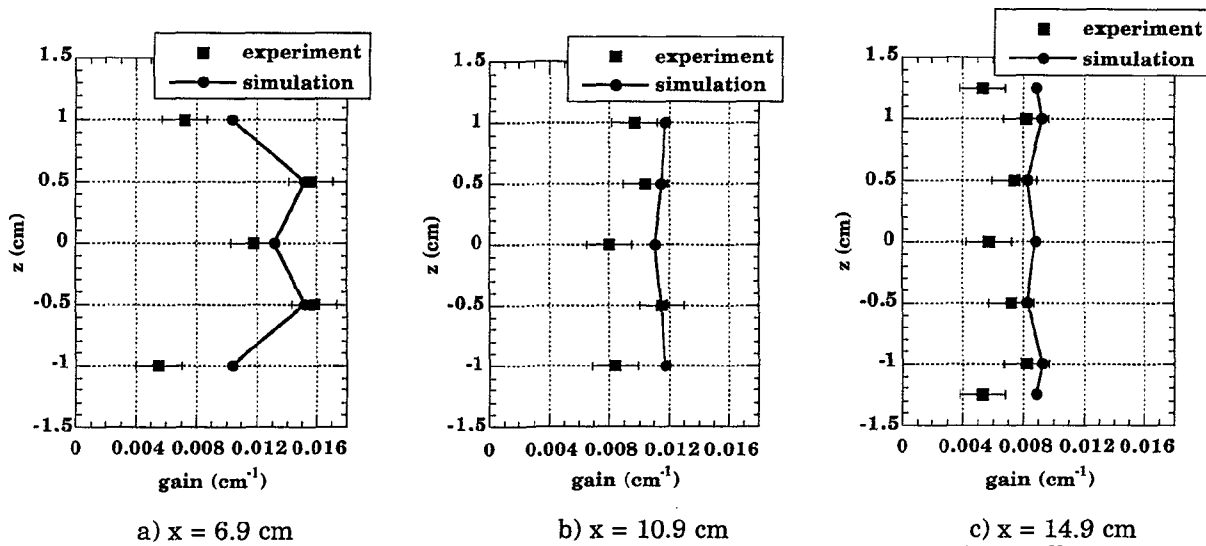


Figure 11. Comparison of average gain from the 126 torr simulation with experimentally measured gain at different streamwise positions.

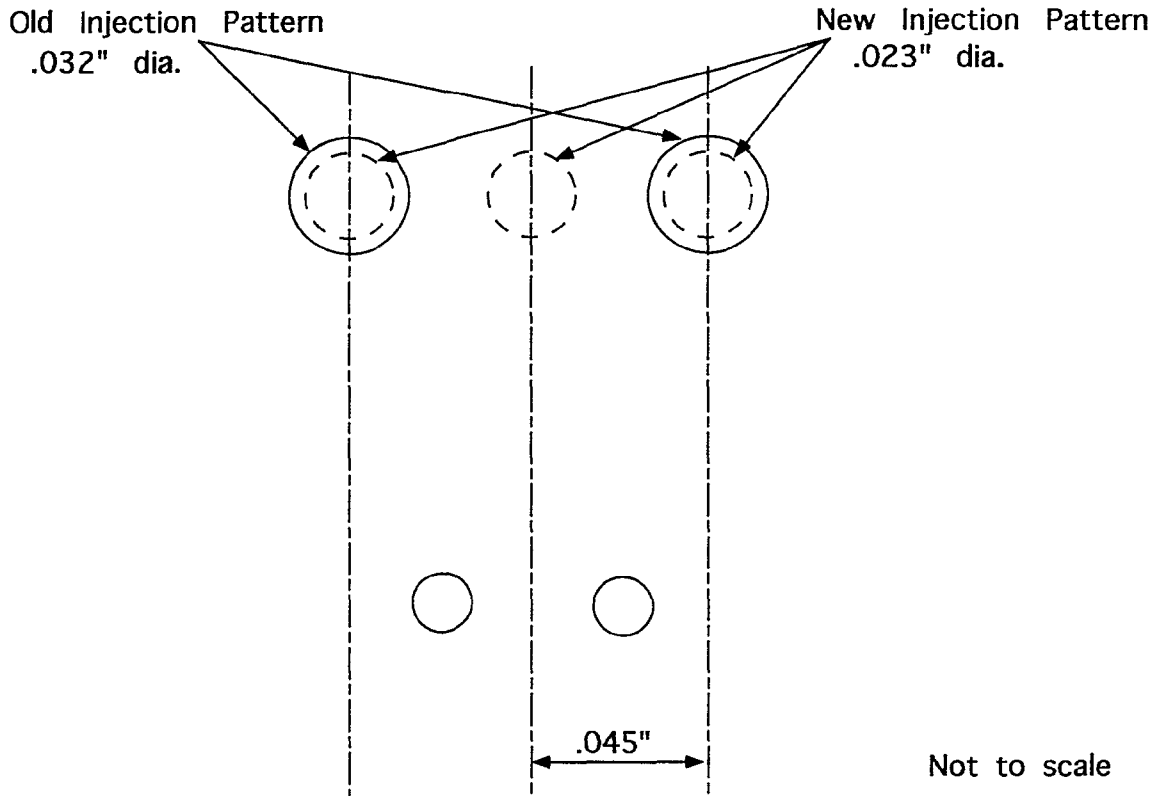


Figure 12. Comparison of original and new injection schemes.

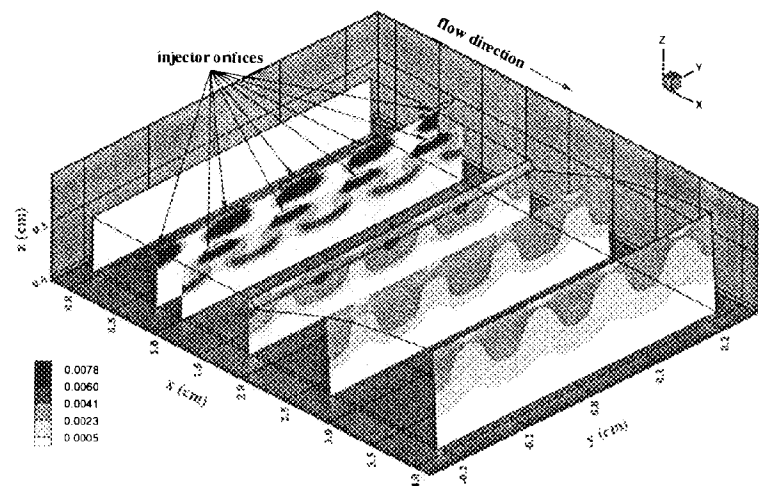


Figure 13. I_2 mole fraction in Zone 1, new injection, 126 torr.

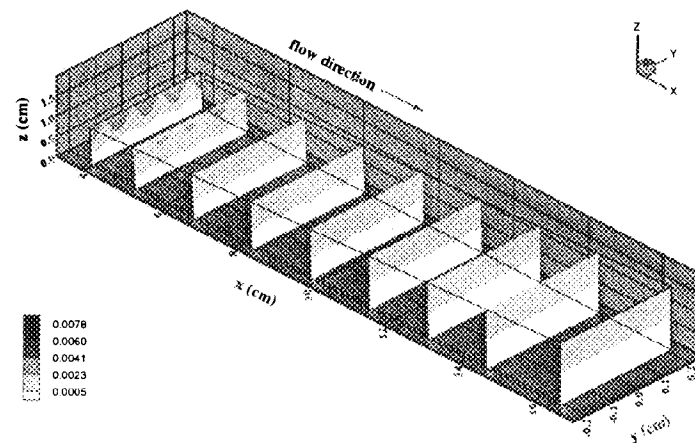


Figure 14. I_2 mole fraction in Zone 2, new injection, 126 torr.

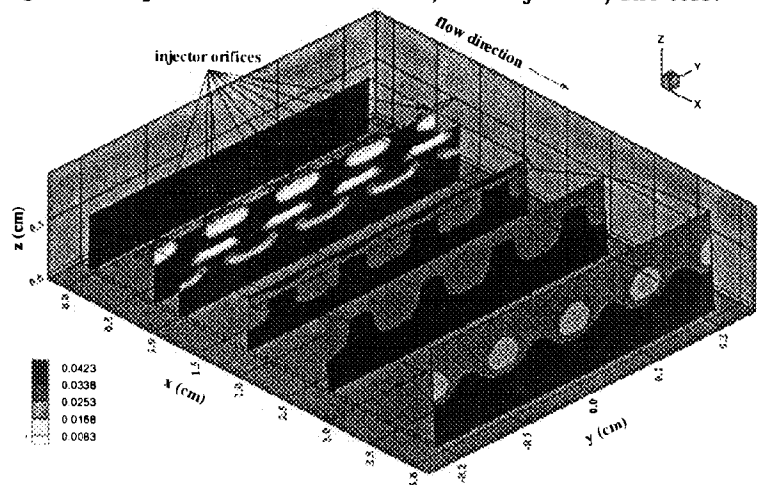


Figure 15. $O_2(^1\Delta)$ mole fraction in Zone 1, new injection, 126 torr.

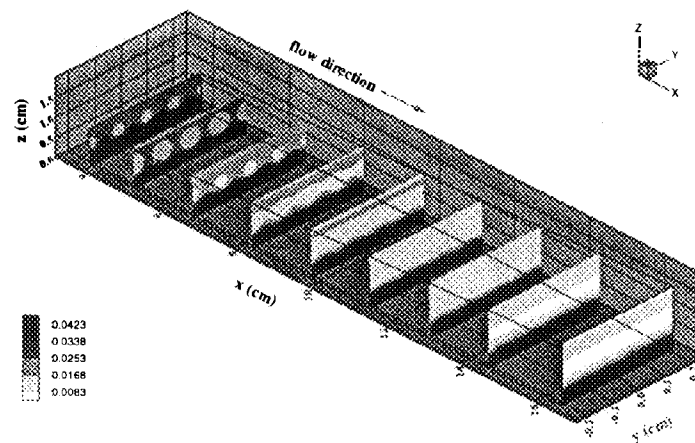
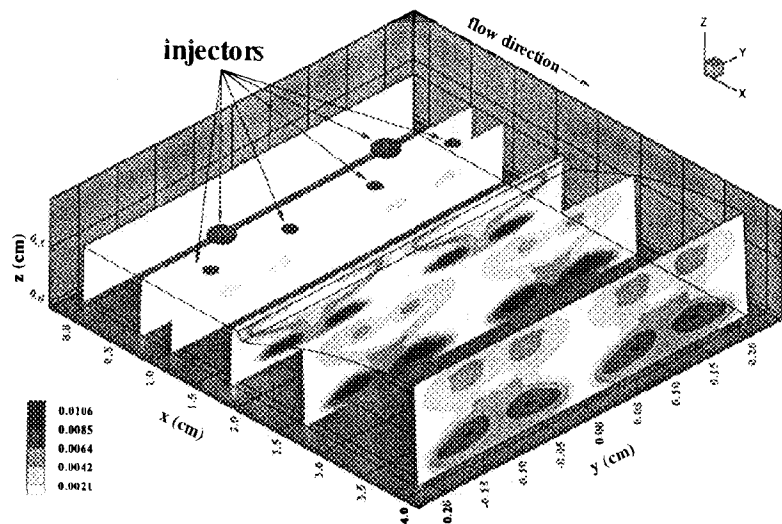
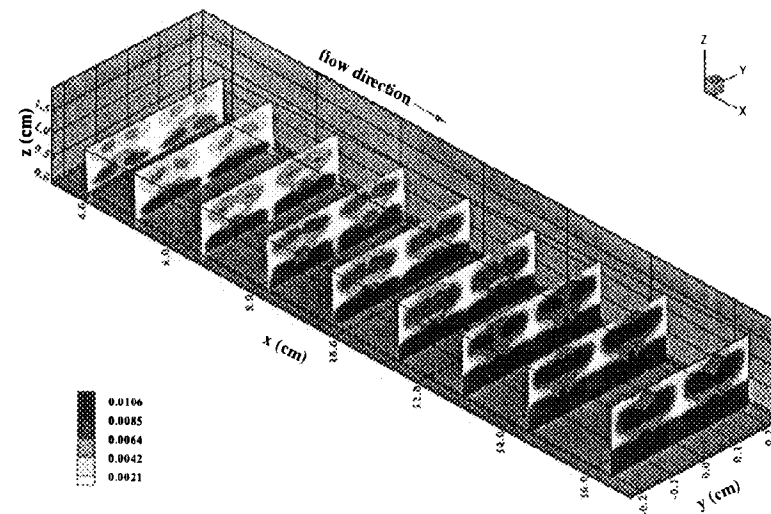


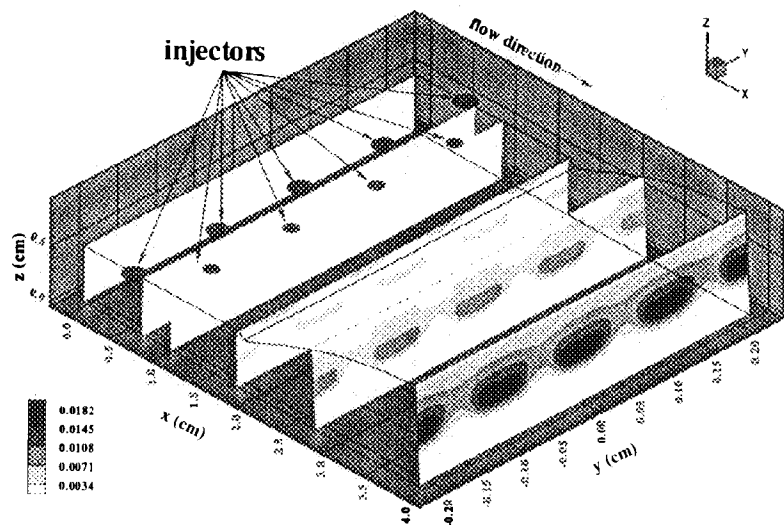
Figure 16. $O_2(^1\Delta)$ mole fraction in Zone 2, new injection, 126 torr.



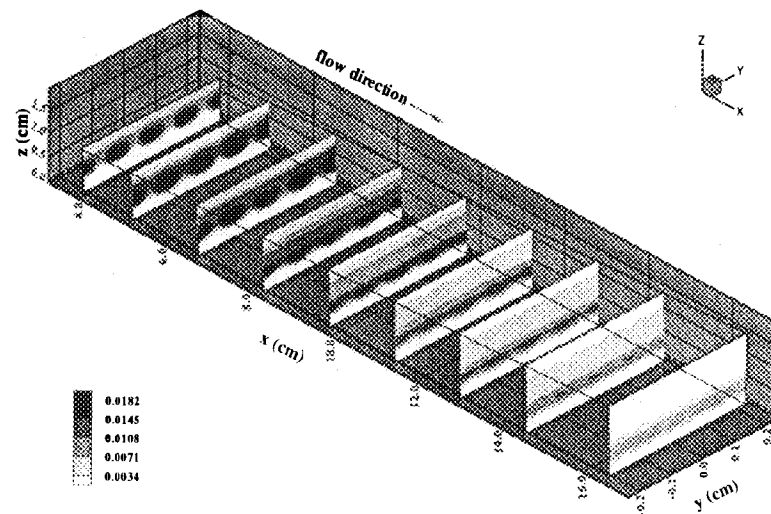
a) Gain(cm^{-1}), zone 1, original injection scheme.



b) Gain(cm^{-1}), zone 2, original injection scheme.



c) Gain(cm^{-1}), zone 1, new injection scheme.



d) Gain(cm^{-1}), zone 2, new injection scheme.

Figure 17. Comparison of gain profiles for original and new injection schemes, 126 torr.